Machine Vision and Applications (1999) 11: 171–190

Machine Vision and Applications

CATALOG: a system for detection and rendering of internal log defects using computer tomography

Suchendra M. Bhandarkar[1], **Timothy D. Faust**[2], **Mengjin Tang**[2]

[1] Department of Computer Science, The University of Georgia, Athens, GA 30602–7404, USA; e-mail: suchi@cs.uga.edu
[2] Warnell School of Forest Resources, The University of Georgia, Athens, GA 30602–2152, USA; e-mail: {tfaust,tang}@arches.uga.edu

Received: 1 August 1997 / Accepted: 25 August 1999

Abstract. This paper describes the design and implementation of a machine vision system CATALOG for detection and classification of some important internal defects in hardwood logs via analysis of computer axial tomography (CT or CAT) images. The defect identification and classification in CATALOG consists of two phases. The first phase comprises of the segmentation of a single CT image slice, which results in the extraction of 2D defect-like regions from the CT image slice. The second phase comprises of the correlation of the 2D defect-like regions across CT image slices in order to establish 3D support. The segmentation algorithm for a single CT image is a complex form of multiple-value thresholding that exploits both, the prior knowledge of the wood structure within the log and the gray-level characteristics of the image. The algorithm for extraction of 2D defect-like regions in a single CT image first locates the pith of the log cross section, groups the pixels in the segmented image on the basis of their connectivity and classifies each 2D region as either a defect-like region or a defect-free region using shape, orientation and morphological features. Each 2D defect-like region is classified as a defect or non-defect via correlation across corresponding 2D defect-like regions in neighboring CT image slices. The 2D defect-like regions with adequate 3D support are labeled as true defects. The current version of CATALOG is capable of 3D reconstruction and rendering of the log and its internal defects from the individual CT image slices. CATALOG is also capable of simulation and rendering of key machining operations such as sawing and veneering on the 3D reconstructions of the logs. The current version of CATALOG is intended as a decision aid for sawyers and machinists in lumber mills and also as an interactive training tool for novice sawyers and machinists.

Key words: Automated log inspection – Automated lumber grading – Computer tomography – Non-destructive evaluation – Non-destructive quality assessment

Correspondence to: S.M. Bhandarkar

1 Introduction

Internal features of hardwood logs such as knots, cracks, decay and other anomalies of tree growth determine their ultimate value. If these defects were known prior to the sawing of the log, optimized sawing plans could be devised to achieve greater value from the log. Production of lumber is essentially a destructive process. With each cut into the log, new information is divulged on the quality of the wood inside which often suggests a different and better sawing or cutting pattern. However, since each step in the sawing process is irreversible, the loss in the value yield has already happened and cannot be subsequently rectified. Hardwood lumber production has traditionally had a low conversion efficiency. Haygreen and Bowyer [21] report that an average of 35% of the log is converted to usable lumber. Improving the lumber value yield from logs has become important to many sawmill managers as the cost of logs has risen to 80% of total production costs [22]. Existing technologies to increase lumber volume by external log inspection have reached the point that little further progress is expected. Even today's most experienced sawyers cannot glean from an external inspection of the log, knowledge of its internal features and their location to any degree of accuracy. It seems reasonable to assume that future gains in lumber value yield will be possible only by internal log scanning.

A detailed knowledge of the presence, location, and size of internal defects prior to the first cut into the log is estimated to lead to potential gains of about 15–18% in lumber value [28, 36, 37, 41]. On a national basis this represents a savings of $2 billion for the United States hardwood lumber industry. Hardwood resources continue to be underutilized in many regions of the US [40]. Environmental concerns and the ecological need for maintaining biodiversity in forest ecosystems underscore the need to utilize as many hardwood species for wood products as possible, thereby reducing the pressures on harvesting a few select species. Forest-products-based economies are also dependent on getting the highest value wood products from a declining forest resource base. Improving the efficiency in converting low-grade logs into high-value products would reduce harvesting pressure on select hardwood species. High-value hardwoods such as Hard Maple, Black Walnut, White Ash and Red Oak

have the greatest differences in value between the highest and lowest lumber grades. Improving yields of higher grade lumber via identification and localization of internal defects will significantly increase the value of these scarce hardwood resources. In summary, optimized production of lumber from hardwood logs would maximize the resulting value of hardwood lumber, allow better utilization of hardwood logs, reduce unnecessary wastage and thus play a significant role in the conservation of depleting hardwood forest resources in the US and all over the world.

Studies of computer axial tomography (CAT or CT) and nuclear magnetic resonance (NMR) scanning for internal log defects [7, 17, 22, 29, 41] have demonstrated that both CT and NMR scanners available today can be used successfully to image the internal features of logs. CT scanners, which are essentially solid state (i.e., with no moving parts), can scan at rates exceeding 30 slices per second. Thus the technical feasibility of scanning logs in real time is approaching reality. However, the computational methods for interpreting the CT scans of logs reliably and in real time are an open research topic.

In this paper, we present a system CATALOG (**C**omputer **A**xial **T**omography for **A**nalysis of **LOG**s) for the detection and 3D rendering of internal defects of hardwood logs. CATALOG is also capable of simulating various machining operations on hardwood logs such as sawing and veneering. The current version of CATALOG focuses on the detection and 3D rendering of important defects such as knots, holes, bark/moisture pockets and cracks via analysis of a set of cross-sectional CT images of hardwood logs. We expect the current version of CATALOG to be used as a decision aid by sawyers and machinists in a lumber mill. The detection and rendering of hardwood defects and computer simulation of key machining operations would assist sawyers and machinists to decide on an optimal lumber production strategy for a given hardwood log. CATALOG could also be used as an interactive training tool for novice sawyers and machinists, whereby they could practice various lumber production strategies on *virtual* logs before working on real logs.

2 Review of related work

CT and NMR scanning represent two potentially viable techniques for acquiring cross-sectional images of logs. Although NMR is a more recent innovation, CT technology is approaching the speed necessary for production use [22]. The first CT scanners developed for medical use in the early 1970s, measured X-ray absorption which was then correlated with material density. A brief description of the computational principle underlying CT is explained in [25] and a detailed history and evolution of CT scanners is given in [29]. While CT scanners are currently available for industrial uses such as testing poles and concrete, the CT scanning technology developed for medical use holds the most promise for adaptation to sawmills.

Although NMR scanners became commercially available in the mid-1980s, NMR techniques have been widely used for more than 30 years to study the molecular structures of solid-state materials and chemical compounds. NMR images are characterized by the fact that wet portions of the object being imaged appear as relatively light regions in the resulting image, whereas dry portions of the object appear as relatively dark regions in the image. Hence, NMR imaging techniques are particularly well suited for detecting internal features of logs that are characterized by varying moisture content in the underlying wood [6, 7]. Chang et al. [6] evaluated internal defects of hardwood logs using NMR scanning technology. Defects such as knots, reaction wood, wetwood, and gum spots were clearly identified. The locations of hidden defects such as buried knots and scars were also provided by the images. Information about uneven moisture content distribution was shown to be useful in identifying potential drying problems. Algorithm development was identified as a key requirement to utilizing NMR. Chang [7] also evaluated the economic feasibility of fast NMR imaging scanners in hardwood sawmills. It was shown that once NMR scanning systems could be purchased for less than $1 million, their use in sawmills would become economically feasible [7].

Hodges et al. [22] evaluated the economic potential of CT in hardwood sawmills. For large mills ($60 \times 10^3 m^3$/year), investments in CT scanning systems could be profitable even with only moderate increases in lumber value yield (5–10%), whereas for smaller mills ($12 \times 10^3 m^3$/year), such investments would become profitable only as increases in lumber value yield approached 30%. In their review, Hailey and Swanson [20] evaluated CT and NMR techniques and estimated that the value of solid-wood products could increase by up to 15% from the use of imaging techniques to identify internal defects in logs. They emphasized the need to correlate scanning parameters to internal log characteristics, to advance software and analytical techniques (especially image analysis and computer graphics), and to develop lower priced and portable scanning systems. Funt and Bryant [17] evaluated a computer system that automatically interprets CT images to identify knots, rot, and cracks occurring in logs. It was shown that although CT technology could greatly improve lumber grade and quality, it was critical to reduce algorithm execution times, design larger diameter industrial scanners capable of withstanding typical sawmill conditions, and develop software capable of constructing 3D models from 2D scans. Moisture content variation within the log was identified as a source of error in distinguishing defects from sound wood.

Taylor et al. [39] conducted a feasibility study for locating knots by using industrial photon emission tomography (PET) where the reconstructed PET images were used to identify internal knots and locate the log perimeter. Comparisons between actual log slices and the PET images indicated that both, the log perimeter and knot locations could be accurately identified. However, knot identification could be made difficult by logs with high moisture content and/or relatively uniform densities between knots and surrounding wood. Funck et al. [16] evaluated the potential of machine vision systems to identify defects on wood surfaces. They developed a detailed machine vision database for numerous natural and process-induced surface features of wood relevant to grading and inspection tasks. Algorithms were developed to detect, locate, and classify these features. Wagner et al. [41] used ultrafast CT techniques as a means of acquiring scans at speeds approaching those required to be used in

commercial sawmills and veneer plants. Based upon visual comparisons of crosscut log disks with the corresponding CT images, it was demonstrated that defects can be identified in images taken in ultrafast mode. Wagner et al. [41] also used computer simulation techniques to evaluate the impact of internal log defects on the resulting lumber value. Their results indicated that the use of CT log scanning should result in higher lumber value.

Conners [8] designed a computer vision system to automatically grade hardwood lumber in one step, reducing the need for sequential grading common in many sawmills. This vision system was capable of locating defects within precut boards and also automatically grading the board, using color information to separate clear wood from defects. Conners [9] also discussed a multisensor machine vision system that uses a combination of color imaging, X-ray scanning and laser-based ranging. The X-ray scanner detected knots and other defects, including decay and honeycomb. Laser-based ranging cameras were used to identify additional defects, including wane, splits, checks, and holes, as well as to assist in the interpretation of X-ray images. McMillan et al. [26] evaluated an automatic lumber-processing system ALPS in which logs were scanned by CT to locate internal knots. It was demonstrated that CT images of Southern Pine logs could clearly distinguish between earlywood and latewood zones, pith, juvenile wood, pitch streaks, and knots.

Forrer et al. [14] have evaluated preprocessing algorithms to identify defects in Douglas Fir veneer. Three sweep-and-mark algorithms first gather data by sweeping through an image, then mark regions that might contain defects. Only the information on marked features is used in subsequent algorithms, reducing the amount of data that needs to be processed. The three mark-and-sweep algorithms are based on either statistical features, morphological (shape) features, or spectral features in the form of color clusters. In a related study, Forrer et al. [15] evaluated the performance of three image preprocessing-processing algorithms to identify defects in Douglas Fir veneer. The three sweep-and-mark algorithms operate on the principle of dividing images into tiles, then sweeping through the tiles to determine locations of potential defects using statistical, morphological or spectral features. The study demonstrated that the algorithm that used statistical features provided the best results for identifying log defects such as loose and tight knots, open holes, pitch pockets and streaks. Davis et al. [10], Som et al. [35] and Svalbe et al. [38] describe their efforts at developing a portable X-ray CT scanner capable of scanning telephone and utility poles on site for internal decay. Grundberg and Gronlund [18] describe their efforts at building a database of log images and internal defects for Scotch Pine and Norway Spruce.

Butler et al. [3, 4] investigated a method for detecting veneer defects based on a dual-threshold algorithm. The image was subdivided into tiles which were subsequently marked not only based on their own features (relative to a threshold value), but also based on features of the neighboring tiles which had already been marked. The use of the secondary threshold improved the overall performance of the algorithm, especially on images containing pitch pockets and streaks, and reduced the overall error rate in identifying both clear wood and defects. Samson [30] developed a geometrical model to describe knots within logs and on the surface of lumber beams sawn from those logs. The logs were modeled as perfect cylinders. The knots were modeled as right elliptical cones with apices at the pith and axes at arbitrary angles to the log axis. Samson [31] further developed a mathematical algorithm to describe the effect of knots in the conversion of logs into structural lumber.

More recently, Li et al. [24] and Schmoldt et al. [33, 34] have investigated the use of artificial neural networks for identification and classification of internal defects from CT images of logs. The pixel gray-level value and the gray-level values of its neighboring pixels are fed as inputs to the neural network. The output of the neural network is the classification of the pixel as either a defect or a non-defect pixel. In the former case, the defect pixel is further classified as belonging to a specific defect type such as knot, void, rot, etc. Both, local 2D and 3D pixel neighborhoods were considered as inputs to the neural network. The neural network was shown to have a high rate of correct classification with low miss and false-alarms rates in both cases, with 3D neighborhoods resulting in better performance. However, since only gray-level values are used as inputs, the neural network is reported to have problems distinguishing between knots and moisture pockets, both of which are characterized by high gray-level values in the CT images.

Occena and Schmoldt [27] describe an interactive graphics sawing program GRASP for modeling various hardwood processes such as sawing, veneering and edging. The logs and their internal defects are modeled as closed polyhedral solids, i.e., a set of concatenated polygonal surface patches. Schmoldt et al. [32] describe a veneering simulator for generating and rendering veneer images that result from performing various types of veneer-slicing operations on log CT images. Owing to the limited resolution of the CT images used, the veneer images are fairly coarse. Moreover, no algorithmic details or run-time performance figures are provided.

Zhu et al. [42] describe a prototype computer vision system for identification and localization of defects in hardwood logs using CT images. The system identifies defect-like regions in individual CT images using a multi-threshold algorithm and connects corresponding regions in adjacent CT image slices using a generalization of the 8-neighbor connected-component labeling algorithm. Basic 3D geometric features of the defects are used in conjunction with the Dempster–Schafer theory of evidential reasoning to classify defects. However, statistics on the accuracy and reliability of defect identification and localization are not provided in their paper.

Guddanti and Chang [19] describe a software program TOPSAW for replicating sawmill sawing using CT images of full-length hardwood logs. A log was cut into boards at a local sawmill by letting a sawyer make the sawing decisions. The positions and orientations of the log and the sawblade during the entire sawing process were recorded and then replicated in the TOPSAW program to produce the same boards in the computer. The total value of the boards as estimated by the software matched to within 97% of the value produced at the sawmill. Experimental results on a single hardwood log are reported in their paper.

The CATALOG system, described in this paper, incorporates certain major advances over existing wood- and lumber-processing systems that employ machine vision. CATALOG is an outcome of our earlier research in defect identification in hardwood logs from CT image slices [2, 11, 12]. The current version of CATALOG allows efficient 3D reconstruction and 3D visualization of the log sample. A detailed analysis of the sequence of cross-sectional CT images of the log sample results in the generation of a 3D model of the log sample that incorporates both (i) the 3D characterization of the internal defects and (ii) the 3D characterization of the ring structure of the log sample. Unlike GRASP [27], CATALOG uses a volumetric model which is more accurate than the wireframe surface model. The 3D model enables the user to view the log sample from any user-specified orientation and viewpoint and also view the interior of the log sample for any user-specified orientation of the cutting plane. This enables the viewer to evaluate a wide variety of sawing patterns without putting steel to wood. CATALOG can also simulate veneering operations on logs and on flat boards obtained by sawing the logs. The voxel-based 3D log model in CATALOG results in a very realistic rendering. Efficient algorithms for mapping the voxel data to pixel data in the sawing plane or veneering plane result in superior run-time performance.

The other distinguishing feature of the CATALOG system is that, like the system of Zhu et al. [42], it explicitly uses the reconstructed 3D information for classification and characterization of wood defects. During the course of design and implementation of CATALOG, we discovered that the identification and classification of certain defects could not be done reliably in a single 2D CT image and that 3D information was necessary to resolve the resulting ambiguity. A majority of wood defect classification systems that rely on 2D CT image data alone tend to be conservative in their classification of defects, i.e., if there is any doubt whether a certain region in the CT image is a defect or not, it is labeled as a defect. This results in a large false-alarm rate. In CATALOG, if a 2D defect does not have adequate 3D support from adjacent 2D image slices, then it is not classified as a defect, thus reducing the false-alarm rate without sacrificing defect detection and classification accuracy. Using information from the 3D reconstruction of the log to resolve and correct ambiguities in the segmentation of the individual 2D CT images is one of the novel features of CATALOG. A major difference between the approach followed in CATALOG and that Zhu et al. [42] is that CATALOG employs a two-stage approach: generation of a defect hypothesis using 2D information from single CT image slices and verification of the hypothesis using 3D information. The system of Zhu et al. [42], on the other hand, uses the 3D information directly for hypothesis generation and hypothesis verification. We have found the approach in CATALOG to be computationally more efficient, since the 3D information is used only in the hypothesis verification stage.

In the sections that follow, we describe the salient features of CATALOG and present experimental results on CT images of real hardwood logs. Section 3 gives an overview of the CATALOG system. In Sect. 4, the segmentation of a single CT image is described. In Sect. 5, the procedure for identification and localization of defects in a segmented CT image is described. Section 6 describes the 3D analysis procedure for verification and correction of the 2D segmentation via correlation across CT image slices and its impact on the performance of CATALOG. Section 7 describes the algorithms for simulation and rendering of key machining operations in CATALOG. In Sect. 8, run time results are presented and the paper is concluded in Sect. 9 with an outline for future research.

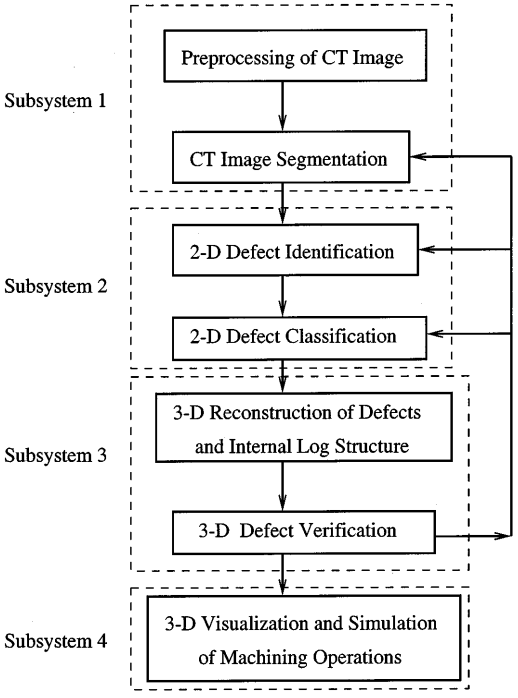

Fig. 1. The high-level structure of the CATALOG system

3 The CATALOG system

The current version of CATALOG consists of four principal subsystems.

(1) Preprocessing and segmentation of individual 2D CT image slices.
(2) Detection and classification of internal defects in the individual 2D CT image slices.
(3) 3D reconstruction of the internal defects and the internal structure of the log.
(4) Simulation of machining operations on the 3D reconstruction of the log.

Figure 1 depicts the overall structure of the CATALOG system. Figure 2 depicts a detailed flowchart describing the various components within the first three subsystems mentioned above. The CT images of the logs were captured using a Toshiba TCT 20AX CT scanner, which has a pixel resolution of 0.75×0.75 mm and a scanning pitch of 5 mm. Each CT image is 320×320 pixels in size with an intensity resolution of 8 bits per pixel (i.e., 256 gray levels). Thus, a log segment of length 1 m produces 200 images resulting in a total of $200 \times 320 \times 320 \approx 19.5$ MB of raw image data. The current version of CATALOG focuses on four representative hardwood species: White Ash, Red Oak, Black Walnut

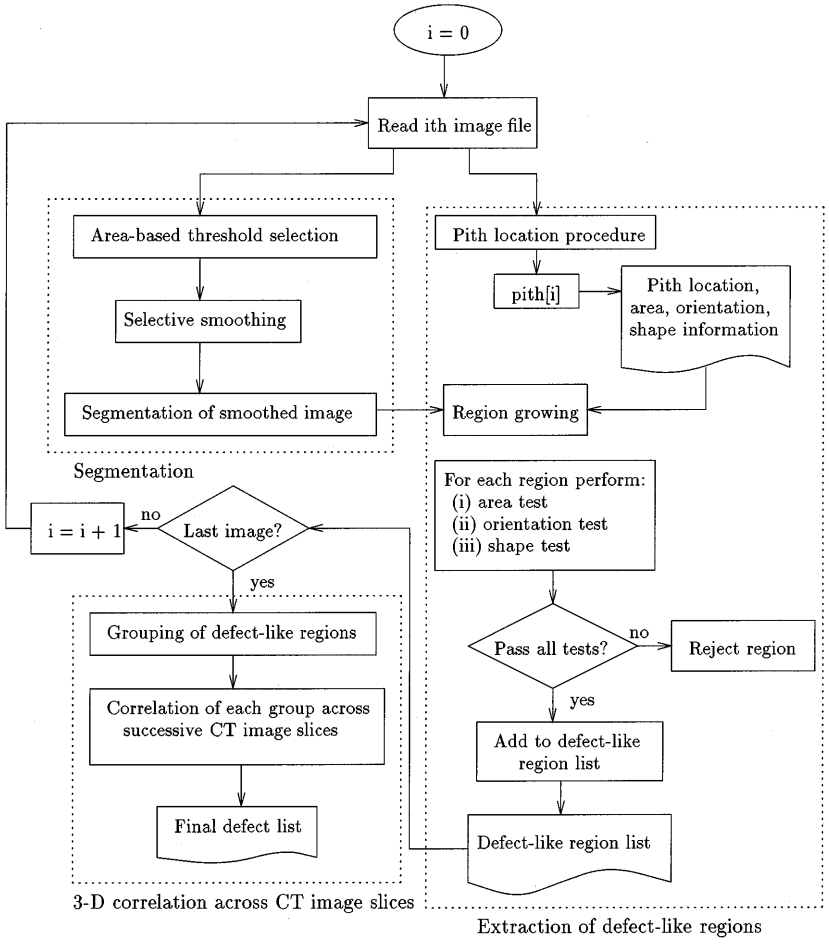

Fig. 2. Flowchart of the defect detection and classification procedure in CATALOG

and Hard Maple. These species account for over 80% of the hardwood lumber production in the United States.

In the initial stages, the defect detection and classification procedure in CATALOG adopts a bottom-up processing approach. It first processes and analyzes each CT image individually and then correlates the results from each CT image with those from neighboring CT images to extract and classify the relevant 3D defects. The knowledge of the 3D internal defects and the growth ring structure deduced from the individual CT image slices is used to reconstruct a 3D model of the internal defects and the internal structure of the log. As depicted in Fig. 1, the reconstructed 3D model is used to detect and rectify errors in the segmentation and classification of the defects in the 2D CT image slices. This ability for top-down verification and error rectification is one of the salient features of CATALOG which sets it apart from other existing computer vision systems for log inspection and lumber grading. The four subsystems in CATALOG are elaborated upon in the following sections.

4 Segmentation of a single CT image in CATALOG

The pixel gray level in a CT image represents the X-ray attenuation coefficient (which is proportional to the amount of X-ray energy absorbed) and consequently the average density (or specific gravity) of the material within the 3D volume representing that pixel. Figure 3 shows sample cross-sectional CT images of logs from the aforementioned four hardwood species. Lower material density results in lower gray-level pixel values in the CT image and vice versa. The density of the wood within a cross section of a log of a given species exhibits significant variation depending on the growth ring structure and the presence of certain characteristic defects within the log. The gray-level distribution of different log slices of the same species was seen to be very similar. Figures 4 and 5 show the gray-level profile along a horizontal line passing through the center of the CT image. Figure 4 shows the gray-level variation caused by the ring structure in White Ash, whereas Fig. 5 shows the gray-level variation caused by the presence of knots in White Ash.

4.1 Gray-level variation in CT images due to wood structure

The significant gray-level variations observed in a CT image slice that is free of defects could be attributed to the following elements of wood.

4.1.1 Ring structure

The ring structure is composed of alternating layers of latewood and earlywood. Since latewood is composed of smaller

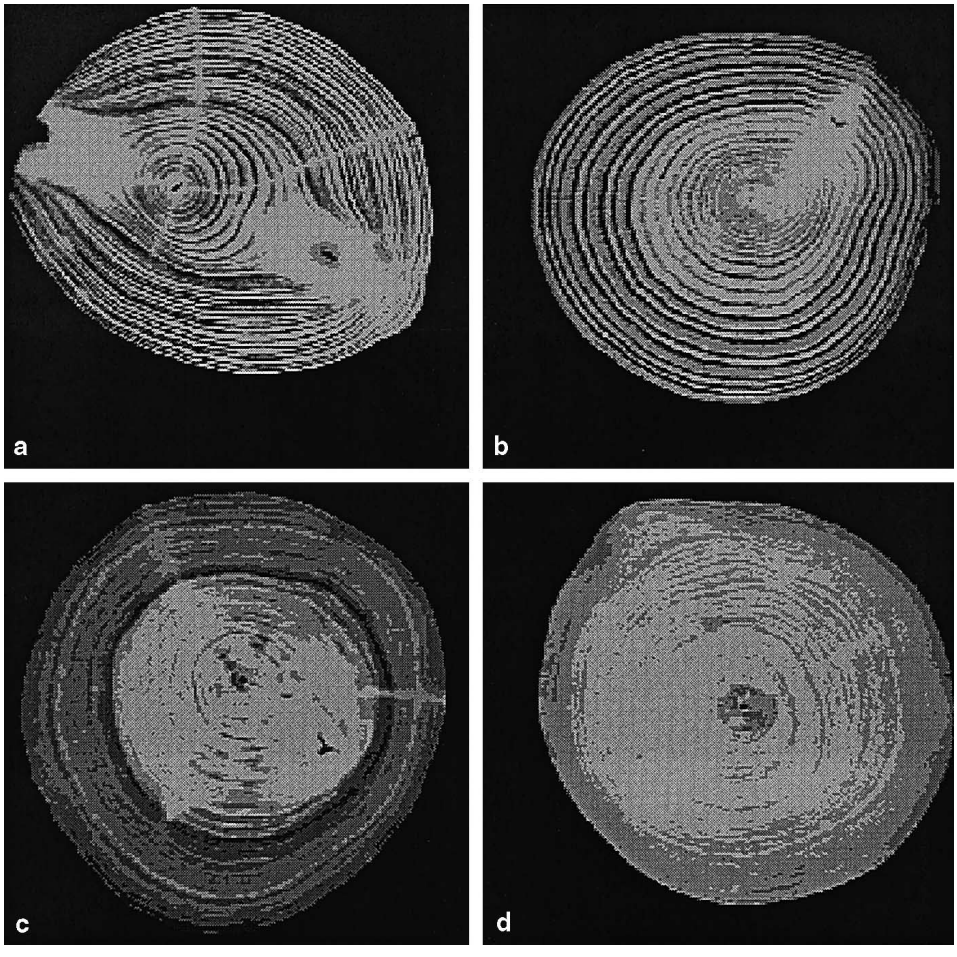

Fig. 3a–d. Sample cross-sectional CT images of **a** White Ash **b** Red Oak **c** Black Walnut **d** Hard Maple

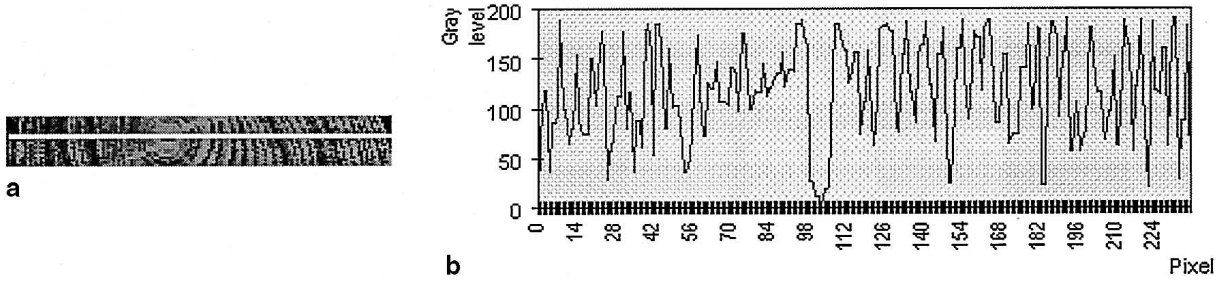

Fig. 4a,b. Gray level variation due to the ring structure in the CT image of White Ash. **a** Portion of the CT image. **b** The gray level profile along a horizontal line passing through the center of **a**

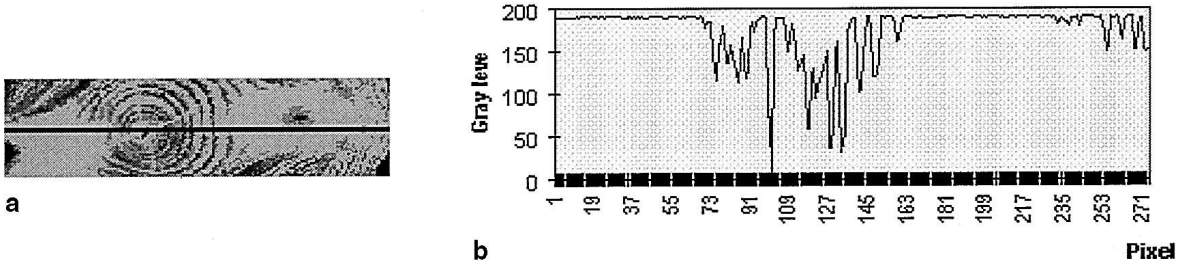

Fig. 5a,b. Gray-level variation due to knots in the CT image of White Ash. **a** Portion of the CT image. **b** The gray-level profile along a horizontal line passing through the center of **a**

size cells it has a higher density than earlywood and appears brighter in the CT images. The ring structure can be modeled as a series of concentric ellipses in the absence of defects. Certain defects such as knots distort the normal ring structure. Thus, if an image region has several broken and/or distorted rings, it may be deemed to contain potential defects.

4.1.2 Sapwood and heartwood

In some hardwood species such as Red Oak and Black Walnut, a pale-colored inner core called heartwood surrounded by a darker outer zone called sapwood can be observed. Heartwood has higher density than sapwood because of higher moisture content and concentration of certain inorganic and extractive materials [21]. Note that, since water has a higher material density than wood, regions of high moisture content appear brighter in the CT image.

4.1.3 Bark

The bark tissue surrounding the log cross section has a higher material density due to higher content of moisture and inorganic minerals. Hence, it shows up as a bright ring surrounding the log interior in a CT image slice.

4.2 Gray-level variation in CT images due to defects

The term *defect* in the wood industry refers to any irregularity, imperfection or deviation from normal wood quality that make the wood unsuitable or less desirable for a specific use. Certain defects such as knots and bark pockets arise due to irregularities of tree growth, whereas cracks and decay arise due to cutting of the wood or invasion by foreign organisms.

4.2.1 Knots

A knot is the portion of a branch that is embedded in the wood of a tree trunk. Knots tend to distort the normal growth rings in the tree trunk. Due to the higher density of cells within a knot, it is characterized by high gray-levels in the CT image. Most knots have an elliptical cross section.

4.2.2 Cracks and holes

Cracks and holes have the lowest material density (since they are comprised of air), and hence are characterized by gray-levels close to zero in the CT image.

4.2.3 Bark pockets and moisture pockets

Bark pockets are a result of small amounts of bark tissue embedded in the wood of the tree trunk. Moisture pockets are a result of high concentration of water in certain regions of the tree trunk. Both, bark and moisture pockets, for reasons cited earlier, are characterized by high material density and therefore exhibit high gray-levels in the CT image.

4.2.4 Decay pockets

Regions in the tree trunk which are invaded by decay-causing organisms result in decay pockets. Since decayed wood has a decreased amount of cellulose and lignin, it has a lower material density than normal wood and shows up darker (i.e., with lower gray-levels) when compared to normal wood. The material density of the decay pocket bears a direct relation to the extent of decay.

4.3 Histogram-based thresholding of CT image slices

Based on the characteristics of the wood structure and defects discussed earlier and our empirical observations, we deem a CT image of a log cross section to be typically composed of four groups of gray-level intensity values. From the lowest to the highest gray-level value they correspond to pixels from (1) cracks, large voids (holes) and decay pockets with advanced decay, (2) decay pockets with early stages of decay and earlywood, (3) latewood, and (4) knots, bark pockets and moisture pockets. Note that gray-levels from each of these classes could overlap with those of adjacent classes. A multiple-thresholding algorithm is used for segmenting the CT image into four classes.

4.4 Area-based multiple threshold selection

The gray-level histogram $H[i]$ of the log CT image, which denotes the relative frequency of each gray-level i in the log CT image is typically multi-modal. It is difficult to select multiple thresholds using a standard threshold selection technique [23], even after a smoothing technique is applied to suppress trivial peaks in the histogram. This is because (a) there are too many peaks in the histogram which cannot be suppressed by the histogram smoothing technique and (b) the valleys between histogram peaks are long and flat making threshold selection difficult. We solve this problem by using a very simple threshold selection technique which we term as *area-based multiple threshold selection*. This technique incorporates the following heuristics: (a) the annual rings of wood are not broken, and hence the image does not contain a single large region whose pixel gray-level values lie within a narrow range and (b) the earlywood and latewood constitute a major portion of the image. The multiple threshold selection is done as follows (Fig. 6).

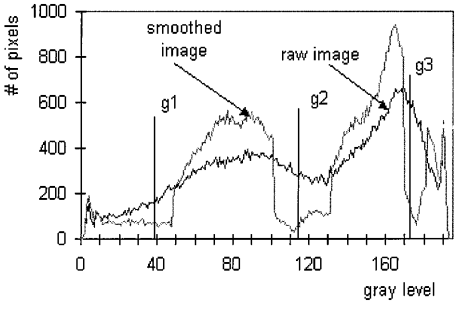

Fig. 6. Histogram of the image and threshold selection

1. Suppose the pixel group with the lowest gray-level range (or the first class) and the pixel group with the highest gray-level range (or the fourth class) account for p_1% and p_2% of the pixels in the log CT image, respectively. As long as p_1 and p_2 are sufficiently large, cracks, voids and decay pockets with advanced decay are assured to be included in the first class and, knots and bark/moisture pockets in the fourth class. On the other hand, the fact that the gray-level values of defects in the first class are significantly lower than the gray-level values of defects in the fourth class prevents the growing of a large connected region that contains both a defect from the first class and a defect from the fourth class (such as a crack and a knot). Also, the risk of adding false positives to the first and fourth classes is small if p_1 and p_2 are chosen to be not too large. Our empirical observations after several experiments have shown values of p_1 in the range 3–5% and p_2 in the range 10–15% to yield good results. We also observed that the results were insensitive to the values of p_1 and p_2 as along as the values were chosen from the aforementioned ranges.
2. Compute the first threshold g_1 as follows:

$$\sum_{i=0}^{g_1} H[i] = p_1 \,. \tag{1}$$

Compute the third threshold g_3 as follows:

$$\sum_{i=g_3}^{Max} H[i] = p_2 \,, \tag{2}$$

where *Max* is the maximum gray-level value in the CT image. The second threshold g_2 is chosen such that

$$\sum_{i=g_1}^{g_2} H[i] = \frac{(100 - p_1 - p_2)}{2} \,. \tag{3}$$

3. Classify each pixel in the CT image as belonging to one of the four classes based on its gray-level value g: Class 1: $0 \leq g < g_1$; Class 2: $g_1 \leq g < g_2$; Class 3: $g_2 \leq g < g_3$ and Class 4: $g_3 \leq g \leq Max$.

4.5 Selective smoothing of the CT image

The CT image of a log contains a fair number of gray-level transitions among earlywood, latewood, and knots. However, since each CT scanner's spatial resolution is limited (ours is 0.75×0.75 mm), a single pixel in the CT image may actually include wood elements from two or more classes, but may only be assigned a gray-level corresponding to a single class. Sometimes a small portion of wood may have abnormal density or may be assigned an incorrect gray value by the scanner (these pixels are termed as noisy pixels). If the thresholds selected above are directly applied to the raw CT image, one may experience the problem of oversegmentation and/or undersegmentation. In an oversegmented image a connected group of pixels arising from a single wood structure may be split into more than one region. In an undersegmented image pixels belonging to distinct wood elements may be incorrectly merged into a single region. This could result in misclassification of normal pixels as defects and also failure to detect certain defects. It is therefore necessary to smooth the CT image to avoid problems of under/oversegmentation. Our selective smoothing algorithm designed for this purpose can be described as follows (Fig. 6).

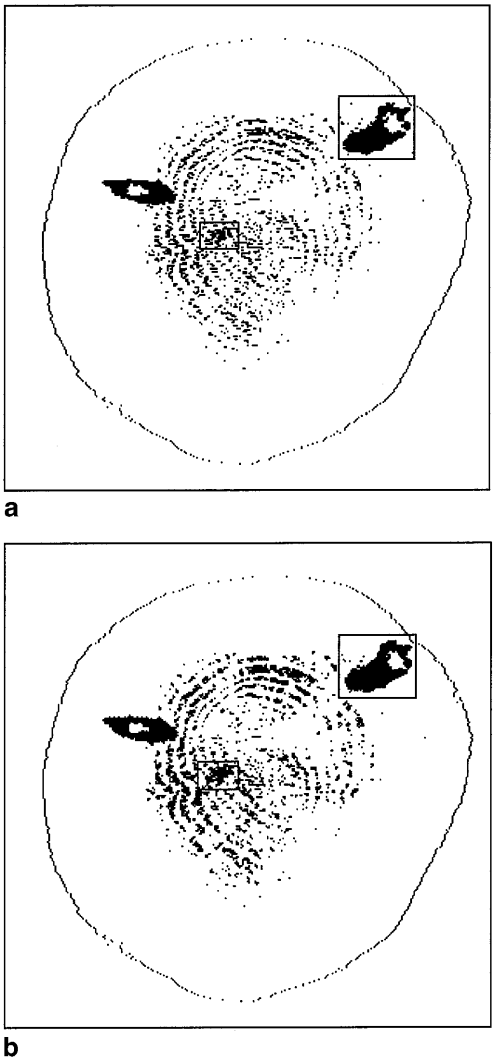

Fig. 7a,b. Pixels from the fourth class: **a** in the raw image; **b** in the smoothed image

1. Suppose the pixel percentages for each transition are known. From these percentages and the gray-level histogram, both the lower gray-level (g_{low}) and the upper gray-level (g_{up}) of each transition are computed.
2. For each pixel with a gray-level value between g_{low} and g_{up}, modify its gray-level by applying a majority filter: if the number of pixels in its 8-neighborhood with gray-level between g_{low} and g_{up} is greater than or equal to 5, then keep its gray-level unchanged, else if the number of pixels in its 8-neighborhood with gray-level less than g_{low} is greater than or equal to the number of pixels in its 8-neighborhood with gray-level greater than g_{up}, set its gray-level to a value lower than g_{low} (typically the average of the gray-level values less than g_{low}), or else set its gray-level to a value greater than g_{up} (typically the average of the gray-level values greater than g_{up}).

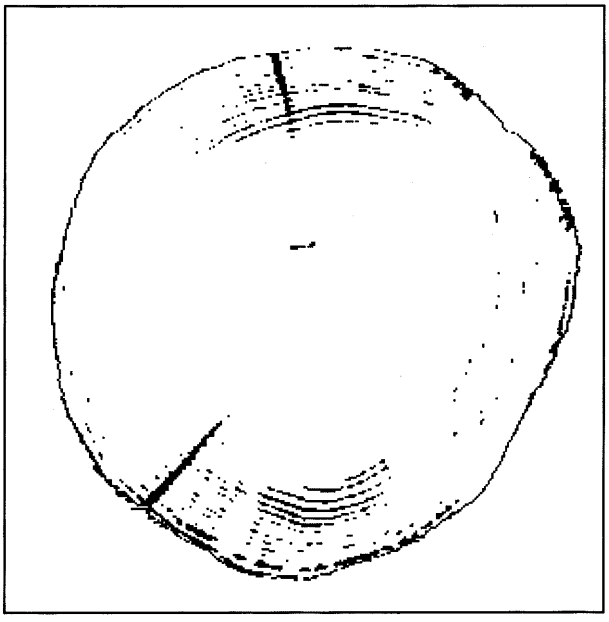

Fig. 8. The pixels from the first class: crack-like defects

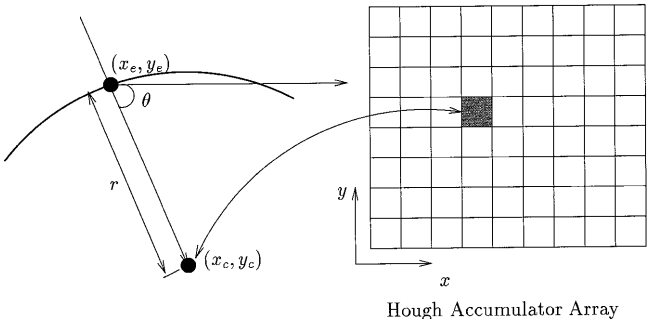

Fig. 9. The Hough transform procedure for locating the pith

Table 1. Results of the pith locating procedure

Species	No. of Images	Percentage of images with pith location precision within		
		5 pixels	10 pixels	20 pixels
White Ash	424	74.2	93.6	96.8
Red Oak	633	60.5	83.0	98.9
Black Walnut	456	83.2	97.8	100
Hard Maple	663	54.5	77.3	99.0

Figure 7 shows the difference between the segmentation results of the original image and the smoothed image. The knot-like region in the upper right corner of the smoothed image has a hole bounded by a closed contour, but not so in the raw image. A small knot near the center of the image can be detected in the smoothed image but probably not in the raw image.

Since the gray value of sapwood is significantly lower than that of heartwood for some wood species, the above selective smoothing technique is not always effective for transitions between earlywood and latewood. In this case, different g_{low} and g_{up} values for earlywood-latewood transitions of sapwood and heartwood may be necessary. But for the purpose of detecting knots, cracks, holes and bark/moisture pockets the aforementioned smoothing algorithm works well.

5 Extraction of defect-like regions from a segmented CT image

After the three thresholds determined in Sect. 4.4 are applied to the smoothed image, the image is segmented into four classes. We ignore the second and third classes because they are mostly comprised of earlywood and latewood. The pixels from the first class in the smoothed image are intended to correspond to cracks and holes and those from the fourth class to knots and bark/moisture pockets (Figs. 7b and 8).

5.1 Locating the pith

The physical pith is a small area which may be viewed as the biological center of a tree although it is rarely located in the geometric center of the log cross sections. It has an important role in aiding the identification of various wood features. For example, growth rings typically form a circular pattern with the pith at the center, and the longitudinal axes of knots and cracks normally pass through the pith.

Assuming that the pith is the innermost portion of the growth rings and that the growth rings are nearly circular in shape, a simple algorithm for locating the pith can be designed. Our algorithm locates the pith using the Hough transform [1] for circle detection. First, the Canny edge operator [5] is applied to the raw CT image and the output thresholded based on edge strength. An edge map denoting the locations of the edge pixels and a gradient direction image are then obtained from the thresholded output. For an edge pixel (x_e, y_e), the coordinates (x_c, y_c) of the center of a circle with radius r within a certain range along the gradient direction θ and passing through the edge pixel are computed as: $x_c = x_e + r\cos\theta$ and $y_c = y_e + r\sin\theta$ (Fig. 9). The corresponding location in a 2D Hough accumulator array representing the x and y coordinates of the centers of the circles is incremented by unity (Fig. 9). The above procedure is repeated for several values of r within a certain range at each edge point. Finally, the location in the accumulator array with maximum value is selected as the location of the pith. In practice, just the central portion of the image (representing about 1/3 of the log cross sectional area) needs to be processed since the pith rarely lies near the boundary of the log cross section. Table 1 summarizes the results of the pith-locating procedure. As can be seen in Table 1, for a majority of the CT images from all the four hardwood species, the pith is localized within a precision of 5 pixels (3.75 mm). For almost all of the CT images from all the four hardwood species, the pith is localized within a precision of 20 pixels (15 mm). An error tolerance of 10 pixels (7.5 mm) in the pith location can be seen to offer a good compromise (Table 1). Subsequent feature detection and localization procedures that rely on the pith location are designed to take this error tolerance into account.

5.2 Identification of defect-like regions

Using a region-growing process, 8-connected pixels (i.e., indirect neighbors and direct neighbors) in the image be-

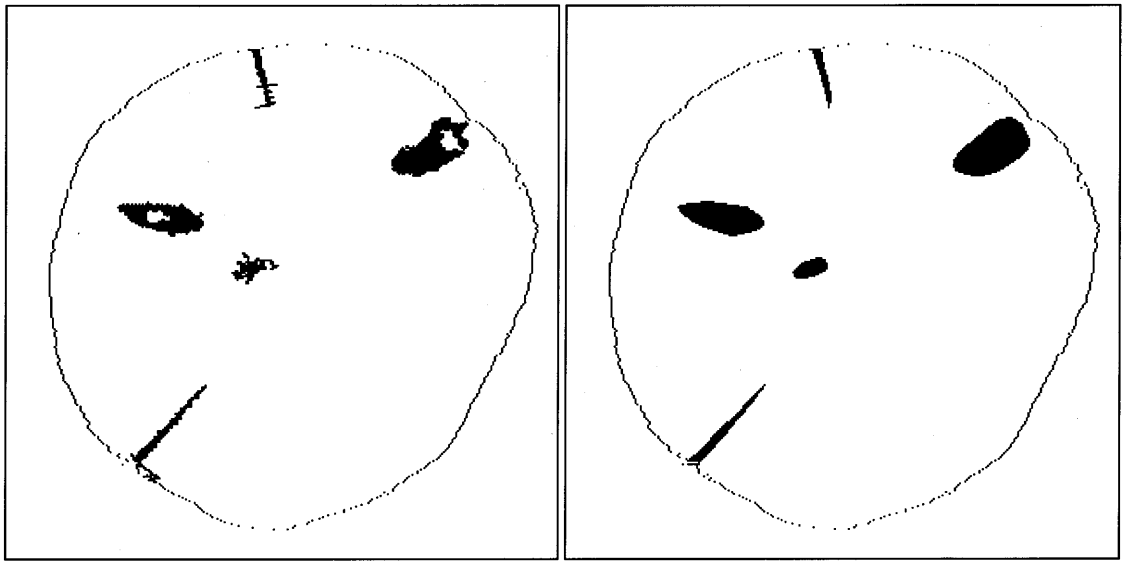

Fig. 10. a Retained defect-like regions with spikes: cracks and knots. **b** The finally retained detect-like regions with holes and gaps filled: cracks and knots

longing to the first class are grouped in the same region, whereas 8-connected pixels belonging to the fourth class are grouped in the same region. For each region R obtained from the region-growing process, the following features are computed.

- Region perimeter P_R, region area A_R and the region centroid (x_R, y_R) computed as $x_R = \frac{1}{A_R} \sum_{(x,y)\in R} x$ and $y_R = \frac{1}{A_R} \sum_{(x,y)\in R} y$.
- Region slenderness S_R which is computed as

  $$S = \frac{I_{max} - I_{min}}{I_{max} + I_{min}},$$

  where I_{max} and I_{min} are the maximum and minimum moments of inertia given by:

  $$I_{max} = \frac{1}{2}\left[M_{20} + M_{02} + \sqrt{M_{11}^2 + (M_{20} - M_{02})^2}\right],$$

  $$I_{min} = \frac{1}{2}\left[M_{20} + M_{02} - \sqrt{M_{11}^2 + (M_{20} - M_{02})^2}\right],$$

  and $M_{ij} = \sum_{(x,y)\in R}(x - x_R)^i (y - y_R)^j$ is the ijth central moment. For all shapes, the value of S_R lies in the range $[0, 1]$, where $S_R = 0$ for a circle and $S_R = 1$ for a straight line segment.
- Region orientation θ_{min} which is the direction of axis of least moment of inertia I_{min} with respect to the x axis. The value of θ_{min} is computed as follows:

  $$\theta_{min} = \frac{1}{2} \arctan\left(\frac{2M_{11}}{M_{20} - M_{02}}\right).$$

  The value of θ_{max} which is the direction of axis of greatest moment of inertia I_{max} is given by $\theta_{max} = \theta_{min} + \frac{\pi}{2}$. Note that θ_{min} and θ_{max} values can be computed only for shapes that are not perfectly circular.

In order to optimize the feature extraction process, a minimum-area criterion was first used to decide whether a region should be retained for further processing or deleted from the region list. A region retained in the list often has some spike-like branches (Fig. 10a) which are deleted using a raster-scan algorithm. For each retained region, the orientations of its major and minor axes are computed as described above. The region's slenderness is used to further classify the defect-like regions from the first class into crack-like regions or hole-like regions. Over the course of several experiments we have empirically determined that holes and bark/moisture pockets have slenderness values in the range $[0.00, 0.40]$, cracks have slenderness values in the range $[0.73, 0.98]$ and knots have slenderness values in the range $[0.13, 0.61]$ for CT images of all the four hardwood species considered in this paper. The contour of the region is then simply represented by the convex hull (for knots, holes and bark/moisture pockets) or a polygon (for a crack). Figure 10b shows the finally retained defect-like regions with holes and gaps filled.

6 3D analysis of defect-like regions across CT image slices

The ultimate objective of the system is to detect 3D log defects from a series of CT images. Therefore, we need to reconstruct 3D defects from the 2D defect-like regions and also verify if they indeed constitute valid defects. Since a log is from a living tree, the physical condition as well as the biological characteristics of the tree may result in a large variation in the CT images of a log. A region in a segmented CT image may be deemed as belonging to a defect, but in reality may be caused by a variation in the physical condition in the wood. For example, consider the CT image of Hard Maple shown in Fig. 11a. The 2D region corresponding to the bright spot in the lower right corner, which in reality was caused by high local moisture content (i.e., a moisture pocket), was incorrectly classified as a knot-like region by the 2D analysis procedure described in the previous section. However, after the log was dried, a CT

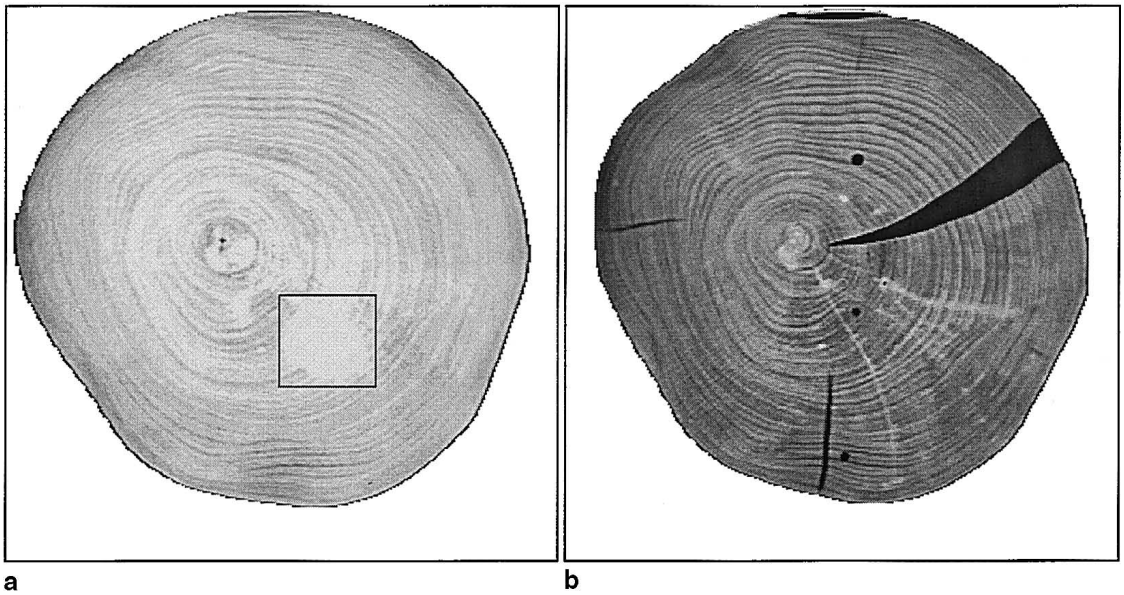

Fig. 11. a The bright spot in the lower right corner in the CT image of Hard Maple is a water pocket misclassified as a knot-like region. **b** A later scan of the dried log sample does not display the bright spot (the cracks were introduced by the drying process)

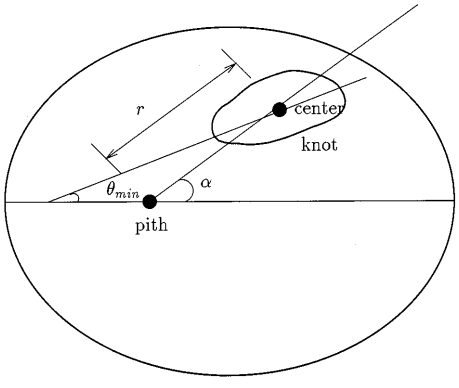

Fig. 12. The geometric parameters used to group the defect-like regions

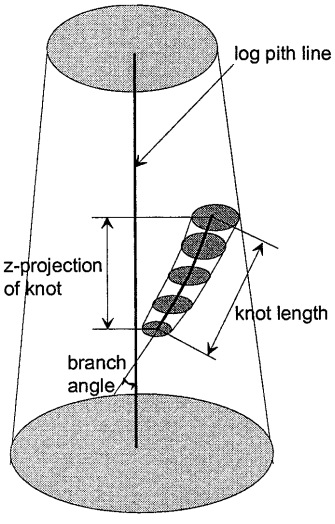

Fig. 13. Branch angle of a knot

image at the same cross sectional location did not display the bright spot (Fig. 11b). Also, when the log was physically cut at the same cross sectional location no knot was revealed.

The above example underscores why it is necessary to discard 2D defect-like regions if they have no 3D support, i.e., have no corresponding defect-like regions in neighboring CT images to constitute a valid 3D defect. Even if a defect-like region has 3D support from neighboring CT images, the defect-like region and the corresponding defect-like regions in neighboring CT images are considered to constitute a *false* defect if they do not satisfy the 3D parameters of a valid defect. In fact, by using knowledge derived from wood science, most ambiguities that arise in the segmentation and classification of defects in 2D CT images could be resolved via 3D analysis of defect-like regions across successive CT image slices.

6.1 Preliminary grouping of defect-like regions

To implement the 3D analysis efficiently, preliminary groups of defect-like regions are generated from the defect-like region list using an iterative clustering procedure with the geometric parameters θ_{min}, r and α depicted in Fig. 12 as features. The parameter r denotes the distance of the centroid of the defect-like region from the pith, whereas θ_{min} denotes the region orientation. Each group is essentially a series of defect-like regions with identical class labels that are spatially connected across CT image slices. A group may be classified as a valid defect if it satisfies a series of 3D tests. In order to optimize the 3D analysis, a group is rejected if the number of 2D regions within it is less than a predefined threshold which is three for a group belonging to the fourth class and ten for a group belonging to the first class. The threshold values are dependent on the minimum size of the defect to be detected, the error tolerance in the pith location and the scanning parameters employed.

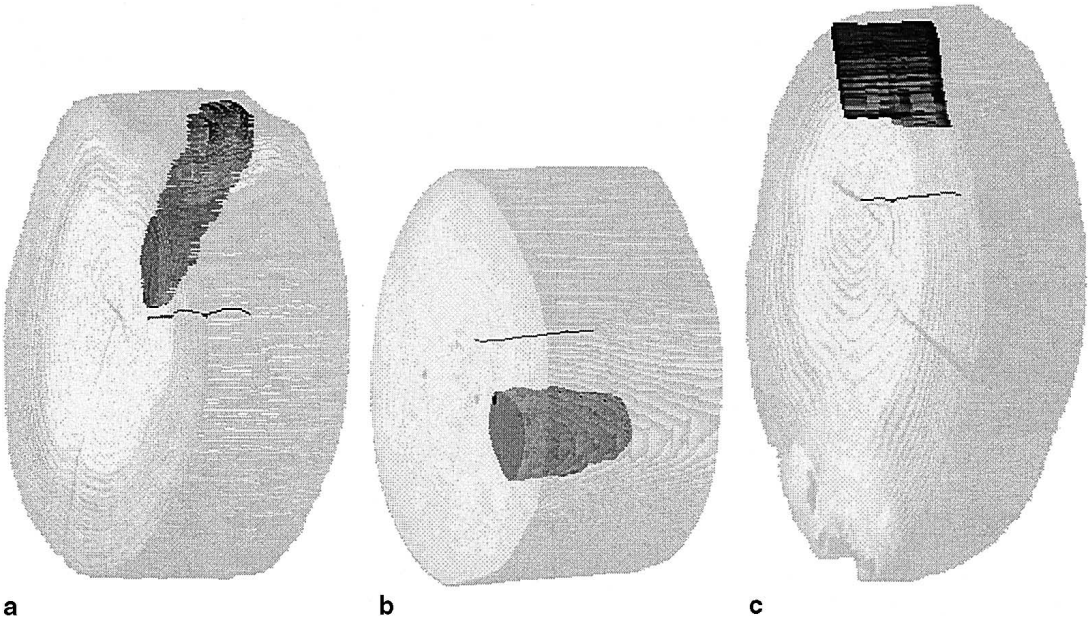

Fig. 14. a A portion of Red Oak shows a knot detected. The branch angle is about 46^o. **b** A portion of Hard Maple shows a water pocket. The angle between pith line and region center line is about 3^o. **c** A portion of Red Oak shows a crack detected

6.2 Measurement of 3D defect parameters using successive CT image slices

A knot is a branch that is embedded in the wood of a tree trunk. The branch angle, which refers to the angle between the branch pith axis and the tree trunk pith axis (Fig. 13) was experimentally determined to be in the range $[30^o, 60^o]$ for all the four hardwood species considered in this paper. Table 2 shows the branch angle values for knots encountered in several CT images derived from all the four hardwood species. The branch angle, measured between the log pith axis and the line passing through the centers of the 2D knot-like regions in successive CT image slices, is the most important factor in distinguishing a knot from other defects belonging to the fourth class, such as a bark/moisture pocket (Fig. 14a and b). For bark/moisture pockets, on the other hand, the angle between the log pith axis and the line passing through the centers of the corresponding defect-like regions was experimentally found to lie in the range $[0^o, 15^o]$. Other slightly less important 3D measurements to distinguish knots from bark/moisture pockets include the change in region area across successive CT image slices, and the region shape. For a normal knot, the area should change from small to large to small along successive CT slices containing the knot, and the region shape is oval with a slenderness factor in the range $[0.13, 0.61]$. For bark/moisture pockets, there is little change in region area and the region shape has a slenderness factor in the range $[0.00, 0.40]$.

For defect groups from the first class, a 3D orientation measurement and the measurement of the angle between the log pith axis and the line passing through the region centers in successive CT image slices are used to determine the validity of the group. The 3D orientation test for a typical crack shows that the plane containing the major axes of the crack-like regions in successive CT slices intersects the log pith axis. The line passing through the region centers in successive CT image slices, on the other hand, is roughly parallel to the log pith axis making an angle in the range $[0^o, 10^o]$ with the log pith axis (Fig. 14c) and with the region shape having a slenderness factor in the range $[0.73, 0.98]$. Since cracks and holes have similar gray-levels, the region slenderness factor is the main distinguishing feature. Holes, typically, were found to have a region slenderness factor in the range $[0.00, 0.40]$.

Table 2. Branch angle and length for knots of four hardwood species

Species	CT image slice nos.	Branch angle (deg)	Knot length (mm)
White Ash	31–44	42.1	66.0
	33–56	45.2	87.1
	81–92	38.3	44.1
	104–130	33.7	159.0
	105–135	33.1	183.5
Red Oak	1–4	52.2	24.6
	14–17	49.1	23.7
	21–43	44.2	143.0
	41–52	47.0	81.5
	121–138	48.1	120.3
Hard Maple	10–23	37.9	80.8
	15–19	34.1	24.8
	20–24	38.3	27.3
	65–70	41.1	31.1
Black Walnut	123–128	33.2	28.1
	141–144	56.2	29.6
	172–183	37.8	71.8
	202–206	55.8	36.8

6.3 Experimental validation of defect identification and localization procedures

The aforementioned procedures for defect identification and localization were subject to comprehensive and rigorous experimental validation. Two log samples each of White Ash

Table 3. Detection rate and false-alarm rate for knots with 2D analysis

Species	Images	True knots	Detected true knots	Detected false knots	Detection rate	False-alarm rate
White Ash	424	225	203	38	90.2%	15.8%
Red Oak	633	161	134	16	83.2%	10.7%
Black Walnut	456	330	283	110	85.7%	28.0%
Hard Maple	663	194	163	84	84.0%	34.0%

Table 4. Detection rate and false-alarm rate for knots with 3D analysis

Species	Images	True knots	Detected true knots	Detected false knots	Detection rate	False-alarm rate
White Ash	424	225	201	13	89.3%	6.1%
Red Oak	633	161	130	7	80.8%	5.1%
Black Walnut	456	330	275	21	83.3%	7.1%
Hard Maple	663	194	158	23	81.4%	12.7%

Table 5. Detection rate and false-alarm rate for cracks with 2D analysis

Species	Images	True cracks	Detected true cracks	Detected false cracks	Detection rate	False-alarm rate
White Ash	424	112	92	6	82.1%	6.1%
Red Oak	633	8	6	2	75.0%	25.0%
Black Walnut	456	29	22	5	75.9%	18.5%
Hard Maple	663	5	4	2	80.0%	33.3%

Table 6. Detection rate and false-alarm rate for cracks with 3D analysis

Species	Images	True cracks	Detected true cracks	Detected false cracks	Detection rate	False-alarm rate
White Ash	424	112	89	2	79.5%	2.2%
Red Oak	633	8	6	1	75.0%	14.3%
Black Walnut	456	29	21	2	72.4%	8.7%
Hard Maple	663	5	4	1	80.0%	20.0%

and Black Walnut and three log samples each of Hard Maple and Red Oak were used in the validation process. The log samples were approximately 1 m in length owing to the fact that the CT scanner did not allow scanning of logs with length much greater than 1 m. The scanned logs were physically cut at cross sectional locations where the corresponding CT images showed a high incidence of internal defects. The cross sections of the cut logs were imaged with an optical scanner with 24-bit color resolution (i.e., 8 bits each for red, green and blue) and spatial resolution of 100 pixels per linear inch. The defects in the color image were manually identified and delineated and treated as ground truth for the purpose of validation. The CT images and the color images were placed in registration for the purpose of validation.

A verification test was performed to ascertain whether a defect-like region in the CT image had a corresponding region in the color image and vice versa. A correspondence between two defect-like regions was deemed to have been established if (i) the defect-like regions has identical labels (knot, crack, or bark/moisture pocket), (ii) the displacement of the region centroids in the two images was less than a predefined threshold, (iii) the difference in region orientation was less than a predefined threshold and (iv) the overlap factor defined as the ratio of the area of intersection of the two regions to the area of the region as measured in the color image was greater than a predefined threshold. The results of the above procedure are used to compute the detection rate (number of defects in the color image that are identified in the CT image) and the false-alarm rate (number of defects in the CT image that have no corresponding defect in the color image). The goal of a machine vision system would be to maximize the detection rate while minimizing the false-alarm rate. The detection rate and false-alarm rate were computed with 2D analysis only and with 2D analysis followed by 3D analysis for knots, cracks, holes and bark/moisture pockets. The detection rate and false-alarm rate results for knots are tabulated in Tables 3 and 4, whereas the results for cracks are tabulated in Tables 5 and 6. As the results show, the incorporation of 3D analysis results in a drastic reduction in the false-alarm rate at the cost of a very nominal decrease in the detection rate. Figure 15 shows the 3D rendering of the detected internal defects in a log with and without 3D analysis.

The localization accuracy was quantified in terms of the average centroid displacement, average region orientation difference and average overlap factor for each defect type, i.e., knot, bark/moisture pocket, crack and hole. The localization results are tabulated in Table 7. Table 7 shows that holes and cracks are localized with greater accuracy, followed by knots and moisture/bark pockets. This can be attributed to the fact that cracks and holes typically exhibit less variance in terms of both shape parameters and gray-level values than knots and moisture/bark pockets.

7 3D visualization and simulation of machining operations

As mentioned earlier, CATALOG is capable of 3D reconstruction and visualization of the scanned logs and simulation and visualization of key machining operations on logs such as sawing and veneering. In contrast to other lumber-processing simulation systems [19, 27, 32] which use approximate log models (such as wireframe models), CATALOG uses a 3D volumetric log model derived by the stacking of the data and results derived from successive CT images. Consequently, the results of our simulation and visualization algorithms are more realistic. In spite of the large volume of data that needs to be handled, our simulation and rendering algorithms are efficient enough that the run times would be considered acceptable in a real-time lumber production environment.

The graphics simulator in CATALOG is designed to be interactive, flexible and extensible and uses a layered object-oriented software development methodology. As shown in Fig. 16, the graphics simulator consists of four layers: user interface (UI) layer, process layer, object layer and data store layer. The UI layer communicates only with the process layer and takes inputs from the user as the arguments to the object builder. It lets the user select what object to construct, and which data sources to use, and specify viewing conditions and other cutting parameters. The process layer consists of the object builder and graphics renderer. The object builder actually consists of several procedures to build models of a log (with or without defects), and models of board or veneer that would result from processing the log. The graphics renderer consists of procedures for setting up

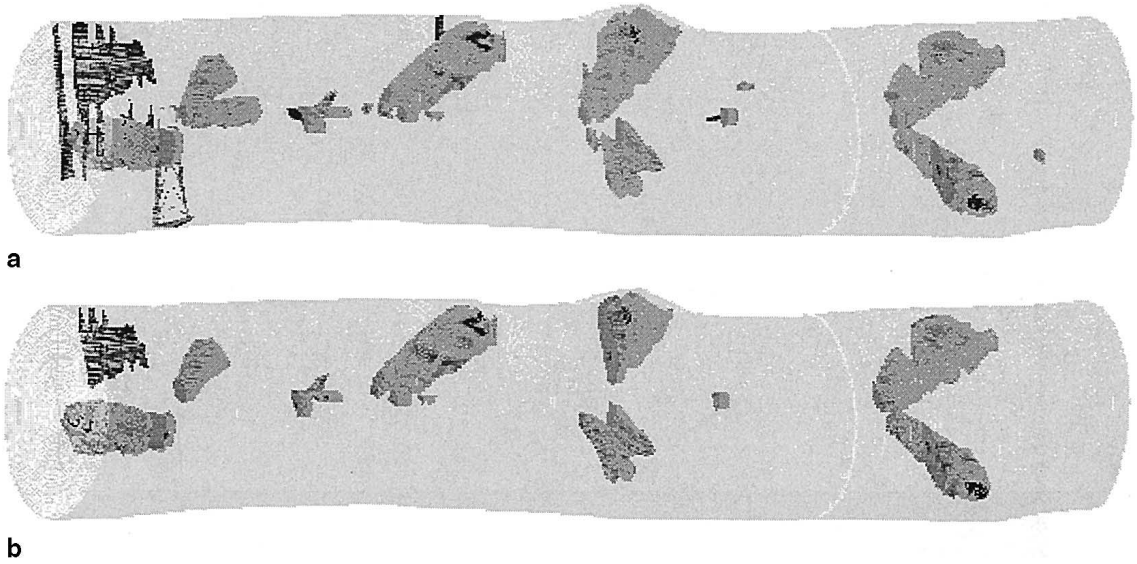

Fig. 15a,b. 3D rendering of the detected internal defects in a log **a** without 3D analysis and **b** with 3D analysis

Table 7. Localization accuracy for internal defects

Defect type	Parameters	Red Oak	Hard Maple	Black Walnut	White Ash
Knot	No. of defects	15	21	20	17
	Centroid displacement (mm)	6.24	3.53	3.11	4.27
	Orientation difference (deg)	8.31	5.54	7.88	6.14
	Overlap factor	0.86	0.83	0.91	0.93
Hole	No. of defects	9	4	2	3
	Centroid displacement (mm)	2.21	1.80	3.82	3.31
	Orientation difference (deg)	10.02	8.81	9.23	5.77
	Overlap factor	0.92	0.97	0.95	0.93
Crack	No. of defects	12	17	7	9
	Centroid displacement (mm)	5.77	3.26	4.29	2.83
	Orientation difference (deg)	6.83	2.87	5.65	4.14
	Overlap factor	0.91	0.93	0.96	0.97
Bark/Moisture pocket	No. of defects	7	3	3	5
	Centroid displacement (mm)	10.34	12.76	8.63	7.42
	Orientation difference (deg)	9.81	9.75	10.22	10.54
	Overlap factor	0.81	0.88	0.83	0.82

the 3D transformations, projections and other viewing parameters. The object layer consists of (i) high-level objects such as the 3D log, 3D defect, sawn product and veneer, (ii) low-level objects describing the volumetric model, surface model and cross sectional boundary of the log, and (iii) raw data which consists of the CT image slices, cutting plane data and cutting line data. The data store layer consists of a file system that stores all the raw data. Future versions of CATALOG will use a database to store raw data.

In the current version of CATALOG, the 3D reconstruction can be viewed in two modes.

(i) The *natural* mode where the log is viewed as a solid entity. This mode allows one to examine the external features of the log.
(ii) The *defect* mode where the defects within the log are viewed as solid entities and the rest of log (including the growth ring structure) is viewed as a semi-transparent entity. This viewing mode is used to highlight the internal 3D defects in the log and also view the relative 3D positions of these defects within the log (Fig. 15).

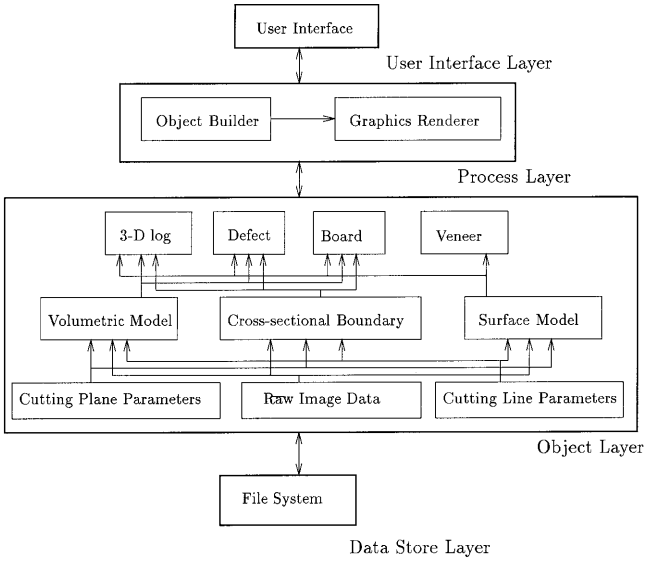

Fig. 16. The graphics simulator subsystem in CATALOG

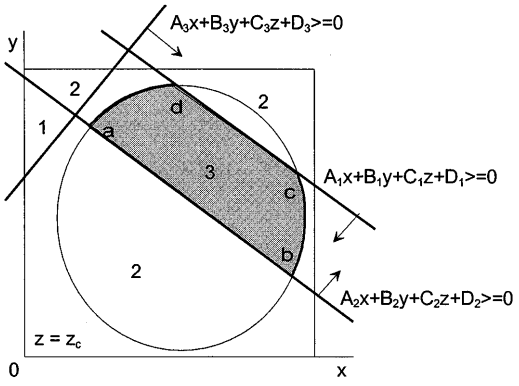

Fig. 17. Cutting planes constraining the sawn product

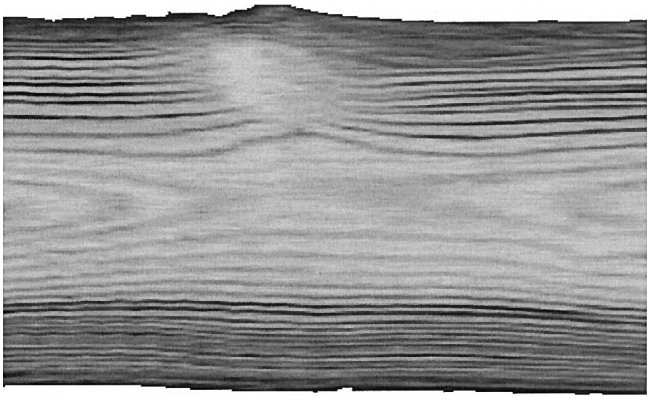

Fig. 18. Result of a simulated sawing operation

In both modes, the user can manipulate the log via translation and rotation in a world coordinate reference frame, via rotation about the log axis and by changing the viewpoint of observation in a world coordinate reference frame or in the log coordinate reference frame. All the above operations are modeled as 3D homogeneous coordinate transforms commonly employed in 3D graphics algorithms [13].

7.1 Simulation of the sawing operation

In CATALOG, a sawn product from a log is modeled as the intersection volume of the log and all the half-spaces defined by the specified sawing planes. In the interest of run-time efficiency, the intersection operation is not performed in 3D space. Instead, the intersection area in each image plane (xy plane with a constant z value) is computed and the results are stacked along the z axis to generate the intersection volume. The cross sectional boundary of the log in each CT image slice is computed using a boundary-following algorithm. The cross section of the sawn product is then computed using the following algorithm.

Algorithm to determine the cross section of the sawn product

Assume that the user has input n sawing planes: $A_i x + B_i y + C_i z + D_i = 0$; $i = l, 2, \ldots, n$. Let each sawing plane define a half-space $A_i x + B_i y + C_i z + D_i \geq 0$ that constrains the sawn product. Let z_c denote the z coordinate of the CT image slice and $ncols$ and $nrows$ the number of columns and number of rows of the image, respectively. Let $AREA$ be the rectangular area defined by $z = z_c$, $0 \leq x < ncols$ and $0 \leq y < nrows$. The intersection operation which determines whether the n half-spaces define a feasible subregion within $AREA$ (Fig. 17) can be computed as follows:

1. Let $ARRAY$ be an array of the same size as $AREA$. All locations in $ARRAY$ are initialized to 0.
2. For each half-space defined by $A_i x + B_i y + C_i z + D_i \geq 0$, do
   a) if the half-space includes $AREA$ or portion of $AREA$, then each element of $ARRAY$ included by the half-space is incremented by 1;
   b) else there is no common intersection for all the half-spaces in $AREA$, hence exit;
3. Compute the intersection region between the pixels in $AREA$ surrounded by the log boundary points (i.e., interior pixels of the log cross section) and the $ARRAY$ pixels with value n (Fig. 17).
4. Stack the intersection regions computed in successive CT image slices to generate the 3D model for the sawn product.
5. Since the resolution along the z axis is much coarser than that along the x and y axes, use linear interpolation along the z axis to improve the visual quality of the model.

For the sawing operation, the user can specify the positions and orientations of the sawing planes, the position and orientation of the log and the viewpoint of observation, each either in a world coordinate reference frame or in the log coordinate reference frame. Once the log is sawed, the user can view the cross section from any viewpoint. The cross section contains both, the markings from the growth ring structure as well as the log defects. Simulation of the sawing operation enables the user to view the 2D boards that would possibly result from subjecting the log to a certain sawing scheme. Figure 18 depicts the result of a simulated sawing operation on a 3D log reconstruction.

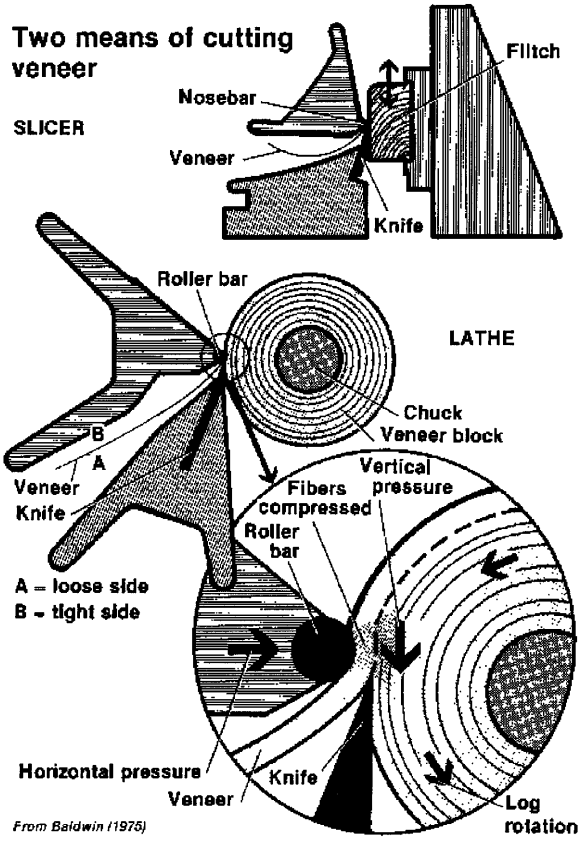

Fig. 19. Veneering operations using rotary-peeling and slicing

7.2 Simulation of the veneering operation

CATALOG is capable of simulating the veneering operation on the 3D log reconstruction as well as on 2D boards that result from the sawing operation. In the former case, the rotary-peeled veneering technique is used where the wood is shaved off the cylindrical surface of the log using a rotary lathe machine. In the latter case, the wood is shaved off the board surface using a slicing machine. Figure 19 depicts both these veneering operations. From a mathematical modeling standpoint, the sliced veneering technique is very similar to the sawing technique discussed previously. Hence, we discuss the rotary-peeled veneering technique in greater detail.

The input parameters for the simulated rotary-peeled veneering operation are: the number of consecutive CT images n, the z coordinates of the first and last CT image slice denoted by z_1 and z_2, respectively, the rotation axis specified by two points $\mathbf{P}_1 = (x_1, y_1, z_1)$ and $\mathbf{P}_2 = (x_2, y_2, z_2)$, the veneer thickness t, and the diameter of the inner core D_{min} (Fig. 20). From the log cross sectional boundary computed for each CT image slice and the specified rotation axis, the maximum diameter D_{max} of the veneering cylinder can be computed (Fig. 20b).

Given the CT image coordinate system (x, y, z), a veneer coordinate system denoted by (x_v, y_v, z_v) is created with its origin at $\mathbf{P}_1 = (x_1, y_1, z_1)$ and z_v axis in the direction $\mathbf{P}_1\mathbf{P}_2$. The transformation between the CT image coordinate system and the veneer coordinate system is given by

$$[x_v, y_v, z_v, 1]^T = \mathbf{R}_y(\alpha)\mathbf{R}_x(\theta)\mathbf{T}_v[x, y, z, 1]^T ,$$

where

$$\alpha = \arctan\left(\frac{-(x_2 - x_1)}{\sqrt{(z_2 - z_1)^2 + (y_2 - y_1)^2}}\right) ,$$

$$\theta = \arctan\left(\frac{y_2 - y_1}{z_2 - z_1}\right) ,$$

$$\mathbf{R}_y(\alpha) = \begin{bmatrix} \cos\alpha & 0 & \sin\alpha & 0 \\ 0 & 1 & 0 & 0 \\ -\sin\alpha & 0 & \cos\alpha & 0 \\ 0 & 0 & 0 & 1 \end{bmatrix} ,$$

$$\mathbf{R}_x(\theta) = \begin{bmatrix} 1 & 0 & 0 & 0 \\ 0 & \cos\theta & -\sin\theta & 0 \\ 0 & \sin\theta & \cos\theta & 0 \\ 0 & 0 & 0 & 1 \end{bmatrix} ,$$

$$\mathbf{T}_v = \begin{bmatrix} 1 & 0 & 0 & -x_1 \\ 0 & 1 & 0 & -y_1 \\ 0 & 0 & 1 & -z_1 \\ 0 & 0 & 1 & -z_1 \\ 0 & 0 & 0 & 1 \end{bmatrix} .$$

Also

$$[x, y, z, 1]^T = \mathbf{T}_v^{-1}\mathbf{R}_x^{-1}(\theta)\mathbf{R}_y^{-1}(\alpha)[x_v, y_v, z_v, 1]^T .$$

Figure 21a shows a trace line for one complete rotation of the rotary-peeled veneer with initial radius of r and an ending radius of $(r-t)$. The length S of the resulting veneer is given by

$$S = \oint ds = \int_0^{2\pi} \left(r - \frac{\alpha}{2\pi}t\right) d\alpha = 2\pi\left(r - \frac{t}{2}\right) ,$$

where $ds = Rd\alpha = \left(r - \frac{\alpha}{2\pi}t\right) d\alpha$ is the incremental arc length (Fig. 21b).

Let $m = \frac{D_{max} - D_{min}}{2t}$ be the total number of rotations that the log can have with veneer thickness t. Let $S_i = 2\pi\left(\frac{D_{max}}{2} - (i-1)t - \frac{t}{2}\right)$ be the length of the veneer generated by the ith rotation. The total veneer length L is given by

$$\begin{aligned} L &= \sum_{i=1}^{m} S_i = \sum_{i=1}^{m} [2\pi(\frac{D_{max}}{2} - (i-1)t - \frac{t}{2})] \\ &= \pi m(D_{max} - tm) \\ &= \frac{\pi(D_{max} - D_{min})(D_{max} + D_{min})}{4t} . \end{aligned}$$

The simulation of the rotary-peeled veneering operation maps the intersection of a rotary cylinder of radius r and a CT image onto a trace line in the veneer image. The algorithm for the simulation of the rotary-peeled veneering operation is given below.

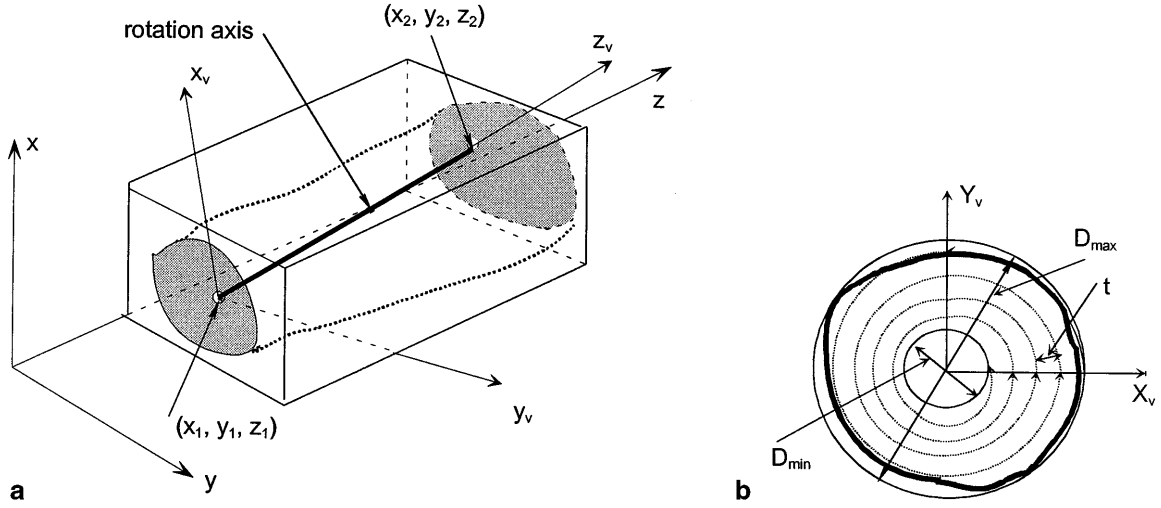

Fig. 20a,b. Parameters for simulation of the rotary-peeled veneering operation. **a** Veneer coordinate system. **b** Rotary peeling parameters

Algorithm for simulation of rotary-peeled veneering operation

1. For $0 < z_v \leq z_c$ (where z_c is the width of the veneer cut), in steps of 1 do
   a) For $D_{max}/2 \geq r \geq D_{min}/2$, in steps of t do
      i. For $0 < \alpha \leq 2\pi$, in steps of $1/r$ do
         A. Compute $x_v = \left(r - \frac{\alpha}{2\pi}t\right)\cos\alpha$.
         B. Compute $y_v = \left(r - \frac{\alpha}{2\pi}t\right)\sin\alpha$.
         C. Compute $[x, y, z, 1]^T = \mathbf{T}_v^{-1}\mathbf{R}_x^{-1}(\theta)\mathbf{R}_y^{-1}(\alpha) \times [x_v, y_v, z_v, 1]^T$.
         D. Determine the gray-level g from the CT image (x, y, z). Use linear interpolation from neighboring pixels in the CT image and from pixels in successive CT slices if necessary.
         E. $I_v[s][z_v] = g$ where I_v is the veneer image and s is the arc length given by $s = \left(r\alpha - \frac{\alpha^2}{4\pi}t\right)$.
2. Display the veneer image $I_v[s][z_v]$. To improve visual quality of the veneer image, supersample it using linear interpolation.

Figure 22 depicts a veneer image generated from a simulated rotary-peeled veneering operation on a 3D log reconstruction. The goal in simulating the veneering operation is to minimize the production of low-grade veneer that contains a lot of defects and thus optimize value recovery.

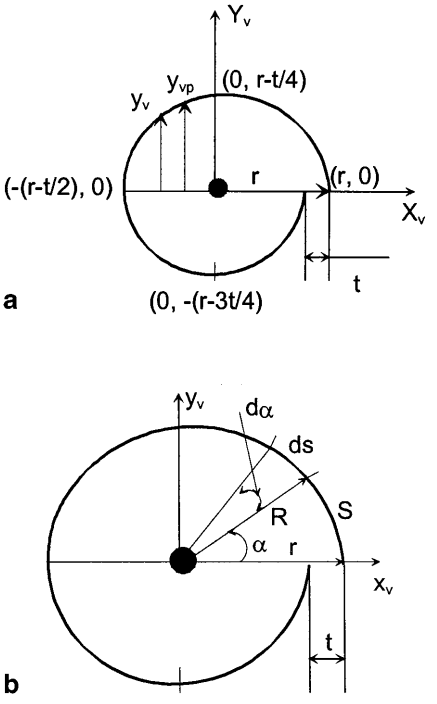

Fig. 21a,b. Computation of the length of a veneer trace. **a** Change of radius during one rotation. **b** Computation of the arc length

8 Run-time results

The algorithms for defect identification, defect localization, 3D model reconstruction, and simulation and visualization of machining operations were implemented in Visual C++ on a 200-MHz PentiumPro workstation with 256 MB of RAM. For the purpose of 3D rendering, a modified version of the z-buffer algorithm was used which allowed for simultaneous rendering of opaque and semi-transparent objects [13]. This was found useful when displaying the reconstructed log in the defect mode.

The defect identification and localization process (with 3D analysis) averaged 112 s on a 1-m-length log which resulted in 200 CT image slices, each of size 320×320 pixels with a gray-level resolution of 8 bits per pixel thus amounting to approximately 19.5 MB of raw image data. The 3D model reconstruction algorithm averaged 57 s whereas the rendering algorithm for the 3D log model averaged 49 s. Overall, the entire process of defect identification, defect localization, 3D model reconstruction and rendering took between 3 and 4 min for all the log species that were considered. The graphical simulation of the sawing operation averaged 38 s for a cut defined by two sawing surfaces. The

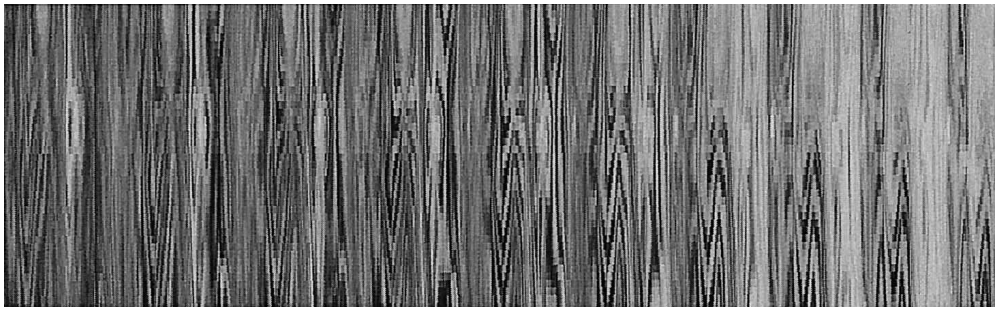

Fig. 22. Veneer image generated from a simulated rotary-peeled veneering operation

graphical simulation of the rotary-peeled veneering operation averaged 8 s for a veneer of length 1.2 m and width of 1 m.

Although the run times mentioned above are impressive, they fall short of those required for real-time processing of lumber in a sawmill. The use of faster hardware is an obvious solution and so is the use of parallel computing. It is to be noted that the processes for defect identification, defect localization and 3D model reconstruction could be pipelined. One could also exploit data parallelism at the pixel level for each of these processes as well as for simulation and visualization of machining operations. Future versions of CATALOG will incorporate these enhancements to make it suitable for real-time processing of lumber.

9 Conclusions and future research

The current version of CATALOG is capable of detection and 3D rendering of defects such as knots, cracks, holes and bark/moisture pockets in hardwood logs of select hardwood species. The species that were considered were Red Oak, Black Walnut, White Ash and Hard Maple, which account for over 80% of the lumber production in the United States. CATALOG is capable of 3D reconstruction and rendering of the log along with its internal defects. CATALOG is also capable of simulating and rendering key machining operations such as sawing and veneering on the 3D reconstructions of the logs. The current version of CATALOG could be used as a decision aid by sawyers and machinists, as well as an interactive tool for training novice sawyers and machinists.

However, the current version of CATALOG does not perform well with CT images containing defects or growth rings with irregular shapes (Fig. 23), containing very dense annual rings, where the width of the rings is less than the scanner spatial resolution, and with CT images that exhibit low-density variation between normal wood and defects. These problems need to be addressed in the future versions of CATALOG.

The future versions of CATALOG will incorporate automated optimal sawing strategy selection and automated lumber grading. The current version of CATALOG relies on the user to select the optimal sawing strategy after having viewed the 3D log reconstruction along with its internal defects, simulated the relevant machining operations on the 3D log reconstruction and viewed the simulation results. The future version of CATALOG will be able to suggest an optimal sawing strategy for the log that would maximize the grade and yield of the resulting lumber and also satisfy the constraints imposed by market demand. We expect this to be a complex problem in computational geometry and constrained optimization. An automated procedure for optimal sawing strategy selection would necessarily entail an automated procedure for lumber grading. Lumber grading would not only have to take into account the presence of defects in the cut lumber but also aesthetic (and hence subjective) aspects based on wood grain texture, wood surface texture, etc. The future version of CATALOG will incorporate a lumber grading rulebase that will be constructed from grading heuristics acquired with the help of expert (human) lumber graders. The use of parallel computing to make CATALOG capable of processing lumber in real time will also be explored.

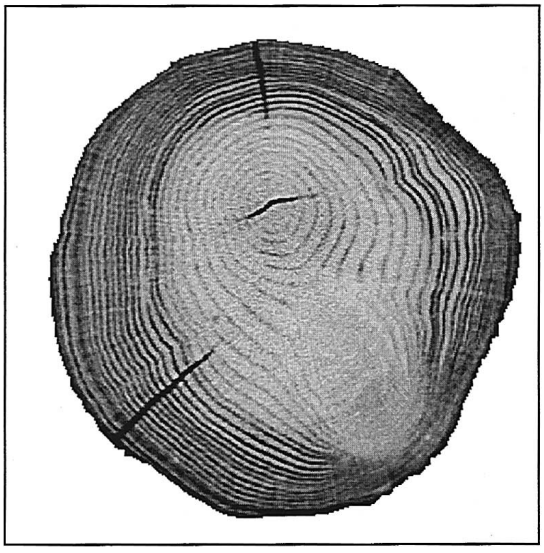

Fig. 23. A CT image of Red Oak with an irregular ring structure

Acknowledgements. This research was partially funded by an NRICGP research grant from the US Department of Agriculture to Dr. Timothy D. Faust and Dr. Suchendra M. Bhandarkar. The authors wish to thank the anonymous reviewers for their insightful comments and suggestions which greatly improved the paper.

References

1. Ballard DH, Brown CM (1982) Computer Vision. Prentice Hall, Englewood Cliffs, N.J.
2. Bhandarkar SM, Faust T, Tang M (1996) A system for detection of internal log defects by computer analysis of axial CT images. In: Proc. IEEE Workshop on Applications of Computer Vision, December 1996, Sarasota, Fla. (IEEE Computer Society Press, Los Alamitos, California), pp 258–263
3. Butler DA, Brunner CC, Funck JW (1989) A dual-threshold image sweep-and-mark algorithm for defect detection in veneer. Forest Prod J 39(5): 25–28
4. Butler DA, Brunner CC, Funck JW (1993) An adaptive image preprocessing algorithm for defect detection in Douglas-fir veneer. Forest Prod J 43(5): 57–60
5. Canny JF (1986) A computational approach to edge detection. IEEE Trans Pattern Anal Intell 8(6): 679–698
6. Chang SJ, Olson JR, Wang PC (1989) NMR imaging of internal features in wood. Forest Prod J 39(6): 43–49
7. Chang SJ (1990) NMR application for internal defect detection. In: Proc. of Process Conrol/Production Management of Wood Products: Technology for the 90s, 1990, Athens, Ga., pp 89–98
8. Conners RW (1987) A computer vision system for grading hardwood lumber. In: Proc. 2nd Intl. Conf. Scanning Technology in Sawmilling, 1987, Oakland, Calif., pp XVI-1–XVI-13
9. Conners RW (1990) A multisensor machine vision system for hardwood defect detection. In: Proc, Process Control/ Production Management of Wood Products: Technology for the ’90s, Annual Meeting, SE Section FPRS, 1990, Athens, Ga., pp 99–111
10. Davis J, Wells P, Benci N, Grant J, McLachlan D (1995) Portable X-ray CT scanner for electricity power pole and tree inspection and a high-resolution laboratory CT system. In: Proc. 2nd International Workshop on Scanning Technology and Image Processing on Wood, 1995, Skelleftea, Sweden, pp 9–22
11. Faust TD, Tang M, Bhandarkar SM, Smith JW, Tollner EW (1996) Evaluation of growth- related features in selected hardwood logs using X-ray computed tomography and image analysis. In: Proc. 10th Int. Sympos. Nondestructive Testing of Wood, August 1996, Lausanne, Switzerland, pp 201–208
12. Faust TD, Tang M (1997) A software system for detection and display of internal defects in logs using axial CT images. In: Proc. Wood Technology Clinic and Show, 1997, Portland, Ore., pp 1–9
13. Foley J, Dam A van, Feiner S, Hughes J (1990) Computer Graphics - Principles and Practice, Second Edition. Addison-Wesley, Reading, Mass.
14. Forrer JB, Butler DA, Funck JW, Brunner CC (1988) Image sweep-and-mark algorithms: Part 1, Basic algorithms. Forest Prod J 38(11/12): 75–79
15. Forrer JB, Butler DA, Brunner CC, Funck JW (1988) Image sweep-and-mark algorithms: Part 2, Performance evaluations. Forest Prod J 39(1): 39–42
16. Funck JW (1990) Softwood Veneer Defect Detection Using Machine Vision. In: Proc. Process Control/Production Management of Wood Products: Technology for the 90s Annual Meet SE Section FPRS, 1990, Athens, Ga., pp 112–123
17. Funt BV, Bryant EC (1987) Detection of internal log defects by automatic interpretation of computer tomography images. Forest Prod J 37(1): 56–62
18. Grundberg S, Gronlund A (1995) The development of a log scanner for Scots Pine. In: Proc. 2nd International Workshop on Scanning Technology and Image Processing on Wood, 1995, Skelleftea, Sweden, pp 40–50
19. Guddanti S, Chang SJ (1998) Replicating sawmill sawing with TOPSAW using CT images for a full-length hardwood log. Forest Prod J 48(1): 72–75
20. Hailey JRT, Swanson JS (1987) Imaging Wood Using Magnetic Resonance. In: Proc. 2nd Intl. Conf. Scanning Technology in Sawmilling, 1987, Oakland, Calif., pp XXVI-1–XXVI-10
21. Haygreen JG, Bowyer JL (1996) Forest Products and Wood Science: An Introduction, 3rd Edition. Iowa State Univ. Press, Ames, Iowa
22. Hodges DG, Anderson WC, McMillin CW (1990) The economic potential of CT scanners for hardwood sawmills. Forest Prod J 40(3): 65–69
23. Kohler R (1981) A segmentation system based on thresholding. Comput Graphics Image Process 15: 319–338
24. Li P, Abbot AL, Schmoldt DL (1996) Automated analysis of CT images for inspection of hardwood logs. In: Proc. IEEE Int. Conf. Neural Networks, 1996, Washington, DC (IEEE Press, Piscataway NJ), pp 1744–1749
25. McMillin CW (1982) Application of Automatic Image Analysis to Wood Science. Wood Sci 14(3): 97–105
26. McMillin CW, Conners RW, Huber HA (1984) ALPS - a potential new automated lumber processing, system. Forest Prod J 34(1): 13–20
27. Occena LG, Schmoldt DL (1996) GRASP: a prototype interactive graphic sawing program. Forest Prod J 46(11/12): 40–42
28. Richards DB (1977) Value yield from simulated hardwood log sawing. Forest Prod J 27(12): 47–50
29. Roder FL, Scheinman E, Magnuson P (1989) High-speed CT scanning of logs. In: Proc. 3rd International Conference on Scanning Technology in Sawmilling, 1989, San Francisco, Calif., pp XV-1–XV-12
30. Samson M (1991) Modeling of knots in logs. Wood Sci Technol 27: 429–437
31. Samson M (1993) Method for assessing the effect of knots in the conversion of I into structural lumber. Wood Fiber Sci 25(3): 298–304
32. Schmoldt DL, Li P, Araman PA (1996) Interactive simulation of hardwood log veneer slid using CT images. Forest Prod J 46(4): 41–47
33. Schmoldt DL, Li P, Abbot AL (1970) Machine vision using artificial neural networks with local 3D neighborhoods. Comput Electron Agric 16: 255–271
34. Schmoldt DL, He J, Abbot AL (1998) A comparison of several artificial neural network classifiers for CT images of hardwood logs. Proc SPIE (Conf. Machine Vision Applications in Industrial Inspection V1) 3306: 34–43
35. Som S, Svalbe I, Davis J, Grant J, Gold E, Tsui K, Wells P (1995) Internal scanning of logs for grade evaluation and defect location. In: Proc. Conf. Digital Image Computing: Techniques and A I . cations (DICTA), 1995, Brisbane, Australia, pp 408–413
36. Steele PH, Wagner FG, Kumar L, Araman PA (1993) The value versus volume yield problem for live-sawn hardwood sawlogs. Forest Prod J 43(9): 35–40
37. Steele PH, Harless TEG, Wagner FG, Kumar L, Taylor FW (1994) Increased lumber value form optimum orientation of internal defects with respect to sawing pattern in hardwood sawlogs. Forest Prod J 44(3): 59–72
38. Svalbe I, Som S, Davis J, Grant J, Tsui K, Wells P (1995) Internal scanning of logs for grade evaluation and defect location. In: Proc. 2nd International Workshop on Scanning Technology and Image Processing On Wood, 1995, Skelleftea, Sweden, pp 1–8
39. Taylor FW, Wagner FG jr, McMillin CW, Morgan IL, Hopkins FF (1984) Locating knots by industrial tomography - A feasibility study. Forest Prod J 34(5): 42–46
40. Forest Service USDA (1988) The South’s Fourth Forest: Alternatives for the Future. Forest Service Report No. 24. Washington, DC
41. Wagner FG, Taylor FW, Ladd DS, McMillin CW, Roder FL (1989) Ultrafast CT scanning of oak log internal defects. Forest Prod J 39(11/12): 62–64
42. Zhu D, Conners RW, Schmoldt DL, Araman PA (1996) A prototype vision system for analyzing CT imagery of hardwood logs. IEEE Trans Syst Man Cybern Part B : Cybernetics 26(4): 522–532

Suchendra M. Bhandarkar received a B.Tech. in Electrical Engineering from Indian Institute of Technology, Bombay, India in 1983, and an M.S. and Ph.D in Computer Engineering from Syracuse University, Syracuse, New York in 1985 and 1989, respectively. He is currently an Associate Professor and Director of the Visual and Parallel Computing Laboratory (VPCL) in the Department of Computer Science at the University of Georgia, Athens, Georgia. He was a Syracuse University Fellow for the academic years 1986–87 and 1987–88. He is a Member of the IEEE, AAAI, ACM and SPIE, and the honor societies Phi Kappa Phi and Phi Beta Delta. He is a coauthor of the book *3-D Object Recognition from Range Images* (Springer Verlag, 1992) and an Associate Editor of *The Computer Journal*. His research interests include computer vision, pattern recognition, image processing, artificial intelligence and parallel algorithms and architectures for computer vision and pattern recognition. He has published over 70 research articles in these areas including over 30 articles in refereed archival journals.

Timothy D. Faust received a B.S. in Forest Products and Forest Science from the Pennsylvania State University in 1978, and an M.S. and Ph.D. in Wood Technology from the University of Georgia in 1983 and 1986, respectively. He was an Assistant Professor and Associate Professor of Wood Technology in the Warnell School of Forest Resources at the University of Georgia from 1986 to 1992 and from 1992 to 1998, respectively. His principal research interests were in production and process control of wood-based manufacturing with emphasis on design and development of computer automated control systems for wood processing environments using machine vision technology. Dr. Faust was a Member of the Forest Products Research Society in which he served as an office bearer in several capacities: Secretary, Treasurer, Student Chapter President, Southeastern Section Chairman and Member of the International Nominating Committee. He was also a Member of the Society of Manufacturing Engineers, American Society of Agricultural Engineers and honor societies Xi Sigma Pi and Gamma Sigma Delta. Dr. Faust had several publications in esteemed journals such as the *Forest Products Journal*, *Wood and Fiber Science* and the *Transactions of the American Society of Agricultural Engineers*. Dr. Faust passed away in December 1998 after a year-long battle with cancer.

Mengjin Tang earned a B.Eng. and an M.S. in Wood Science and Technology from the Nanjing Forestry University, Nanjing, P.R. China in 1982 and 1985, respectively. From 1985 to 1992, he was with the Department of Wood Science and Technology at the Nanjing Forestry University as a research associate and instructor. In 1998, he earned an M.S. in Computer Science and a Ph.D. in Wood Technology from the University of Georgia, Athens, Georgia. Currently, he is a software engineer at Byers Engineering Company, Atlanta, Georgia. His major research interests include automation and optimization of lumber manufacturing, geospatial information processing, and industrial applications of computer vision.